Simulation Study of Nonlinear Magnetohydrodynamic Effects on Alfvén Eigenmode Evolution and Zonal Flow Generation

Y. Todo 1,2), H. L. Berk 3), B. N. Breizman 3)
1) National Institute for Fusion Science, Toki, Japan
2) The Graduate University for Advanced Studies (Sokendai), Toki, Japan
3) Institute for Fusion Studies, University of Texas at Austin, Austin, TX, United States

E-mail contact of main author: todo@nifs.ac.jp

Abstract. Nonlinear magnetohydrodymamic (MHD) effects on Alfvén eigenmode instability and on Alfvén eigenmode bursts were investigated via hybrid simulations of an MHD fluid interacting with energetic particles. The investigation of the Alfvén eigenmode instability focused on the evolution of an n=4 toroidal Alfvén eigenmode (TAE) which is destabilized by energetic particles in a tokamak. In addition to fully nonlinear code, a linear-MHD code was used for comparison. The only nonlinearity in that linear code is from the energetic particle dynamics. No significant difference was found in the results of the two codes for low saturation levels, $\delta B/B \sim 10^{-3}$. In contrast, when the TAE saturation level predicted by the linear code is $\delta B/B \sim 10^{-2}$, the saturation amplitude in the fully nonlinear simulation was reduced by a factor of 2 due to the generation of zonal (n=0) and higher-n ($n \geq 8$) modes. This reduction is attributed to the increased dissipation arising from the non-linearly generated modes. The fully nonlinear simulations also show that geodesic acoustic mode is excited by the MHD nonlinearity after the TAE mode saturation. Furthermore, energetic-particle source, loss, and collisions are implemented in the hybrid simulation code. The energetic particles are simulated using the δf particle-in-cell method with a time-dependent equilibrium distribution function f_0. The first numerical demonstration of Alfvén eigenmode bursts with parameters similar to the TFTR experiment and with MHD nonlinearity retained is presented.

1. Introduction

The destabilization of Alfvén eigenmodes by energetic particles is an important concern for burning plasmas since the excited modes can enhance transport and losses of energetic ions. Computer simulation is a powerful tool to investigate the interaction between Alfvén eigenmodes and energetic particles. We performed the first numerical demonstration of toroidal Alfvén eigenmode (TAE) bursts [1] with parameters similar to a TFTR experiment [2] and many of the experimental characteristics were reproduced. These include: a) the synchronization of multiple TAEs, b) the modulation depth of the drop in the stored beam energy, c) the stored beam energy. However, the saturation amplitude was $\delta B/B \sim 2\times10^{-2}$ which is higher than the value $\delta B/B \sim 10^{-3}$ inferred from the experimental plasma displacement measurements [1, 3]. In the simulation of Ref. 1, the only nonlinearity retained was the nonlinearity in the energetic particle orbits, while the nonlinear magnetohydrodynamic (MHD) effects were neglected. Thus the spatial profiles and damping rates of the TAEs were assumed to be independent of the mode amplitude. Such a simulation is justified when particle trapping is the most important saturation mechanism for the TAE instability [4, 5]. This saturation mechanism has been demonstrated in several previous

simulations [6-9]. However, the linear simulation tends to give too large a saturation level. This suggests that the MHD nonlinearity neglected in the TAE burst simulation may be important and is well worth investigating carefully. In another simulation study of TAE bursts, where the MHD nonlinear effects are taken into account but the parameters are not very close to the experiment, the saturation level is roughly $\delta B/B \sim 5\times10^{-3}$ [10]. The effects of MHD nonlinearities on the increase in TAE damping rate were investigated theoretically [11] and numerically [12]. These studies further motivated us to investigate the nonlinear MHD effects on the TAE evolution to better understand the physics mechanism of saturation.

Recently, we have studied the nonlinear evolution of a single linearly unstable TAE mode with toroidal mode number n=4 [13] using two versions of the MEGA code [14-16] which is a hybrid simulation code for an MHD fluid interacting with energetic particles. With the standard version of the MEGA code, the full nonlinear dynamics of both the MHD fluid and the energetic particles is simulated. In the other version of the MEGA code, only linear-MHD equations are used while the nonlinear particle dynamics is retained. We shall refer to this version as the linear-MHD simulation. A comparison of the results between the nonlinear MHD and linear-MHD simulations is used to clarify how the MHD nonlinearities affect the TAE evolution. Furthermore, the MEGA code has been extended to incorporate energetic-particle source, loss, and collisions. The energetic particles are simulated using the δf particle-in-cell method with time-dependent equilibrium distribution function f_0. The first numerical demonstration of Alfvén eigenmode bursts with parameters similar to the TFTR experiment and with MHD nonlinearity retained is presented.

2. Simulation Model

In the MEGA code, the bulk plasma is described by the nonlinear MHD equations and the energetic ions are simulated with the δf particle method. The MHD equations are solved using a fourth order (in both space and time) finite difference scheme. The drift-kinetic description is employed for the energetic ions. The computational particles are initially loaded uniformly in the phase space. For the purpose of clarifying the nonlinear MHD effects, the linear-MHD calculations were performed. Tokamak plasma with aspect ratio of $R_0/a = 3.2$ was investigated where R_0 and a represent the major radius of the geometrical center of the simulation domain and the plasma minor radius, respectively. The cylindrical coordinates (R, φ, z) are employed. The shape of the outermost magnetic surface is circular. The spatial profiles of the energetic-ion beta, bulk plasma beta and safety factor are shown in Fig. 1 The bulk plasma density is uniform. The different initial values of the central energetic-ion beta β_{h0} were investigated with the profile kept constant. The central energetic-ion beta β_{h0} shown in Fig. 1 is 2.0%. The initial velocity-space distribution of the energetic ions is a slowing-down distribution with a maximum velocity $1.2\mathrm{v}_A$ and the critical velocity $0.5\mathrm{v}_A$, where v_A denotes the Alfvén velocity at the plasma center. The ratio of the energetic-ion Larmor radius to the minor radius is 1/16 for the energetic-ion velocity equal to the Alfvén velocity. The number of grid points for the cylindrical coordinates (R, φ, z) is 128×64×128

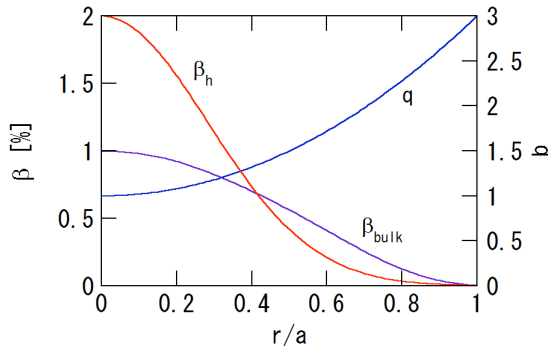

Fig.1 Spatial profiles of energetic-ion beta, bulk plasma beta and safety factor.

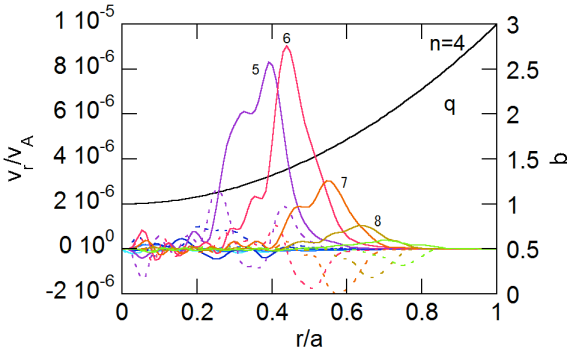

Fig.2 Spatial profile of each poloidal harmonic of the TAE with toroidal mode number n=4 for radial velocity.

and the number of the computational particles is 5.2×10^5. We investigate the evolution of the n=4 mode, which is an exact solution of the equations of a quarter of the tokamak domain with the toroidal angle taken from $0\le\varphi\le\pi/2$. The viscosity, diffusion, and resistivity coefficients in the MHD equations are chosen to be $\nu=\nu_n=10^{-6}\mathrm{v}_A R_0$ and $\eta=10^{-6}\mu_0\mathrm{v}_A R_0$, respectively. The spatial profile of the unstable n=4 TAE mode observed at the linearly growing phase of the instability for $\beta_{h0}=1.0\%$ is shown in Fig. 2. The frequency and growth rate of the TAE are $\omega=0.318\omega_A$, $\gamma=1.3\times10^{-2}\omega_A$ with $\omega_A=\mathrm{v}_A/R_{\mathrm{axis}}$, where R_{axis} is the major radius of the magnetic axis. The maximum values of $\mathrm{v}_r/\mathrm{v}_A$ and $\delta B_r/B$ are close to each other for the TAE.

3. Simulation Results

3.1. Comparison of linear-MHD and nonlinear MHD simulations

The evolution of the MHD radial velocity is compared in Figs. 3 and 4 for the linear-MHD simulation and the nonlinear MHD simulation. A comparison of the radial velocity excitation is made for two different hot particle beta values, $\beta_{h0}=1.5\%$ and $\beta_{h0}=2.0\%$. Figures 3 and 4 show the evolution of the m/n=6/4 harmonics of radial velocity $\mathrm{v}_r/\mathrm{v}_A$ measured at the TAE peak location r=*0.42a*. The frequency and growth rate are $\omega=0.310\omega_A$, $\gamma=3.0\times10^{-2}\omega_A$ for $\beta_{h0}=1.5\%$, and $\omega=0.303\omega_A$, $\gamma=5.1\times10^{-2}\omega_A$ for $\beta_{h0}=2.0\%$. We see in Fig. 3 that the saturation levels of $\mathrm{v}_r/\mathrm{v}_A$ for both the linear-MHD and nonlinear MHD runs are $\sim3\times10^{-3}$ and in the two calculations the phases of the excitation remain synchronized in time, indicating in this case a robust accuracy of the reduced model. On the other hand, for $\beta_{h0}=2.0\%$, a significant reduction of the saturation level can be seen for the nonlinear MHD run in Fig. 4. The saturation level of $\mathrm{v}_r/\mathrm{v}_A$ is $\sim8\times10^{-3}$ for the nonlinear MHD simulation while it is $\sim1.7\times10^{-2}$ for the linear-MHD simulation. The MHD nonlinear effects reduce the TAE saturation level by half when it reaches $\mathrm{v}_r/\mathrm{v}_A\sim\delta B_r/B\sim10^{-2}$. For cases where the instability growth is lower, the saturation level is $\mathrm{v}_r/\mathrm{v}_A\sim\delta B_r/B\sim10^{-3}$, and the MHD nonlinearity does not play any important role. Then the saturation mechanism is dominated by the particle nonlinear dynamics, i.e., the particle trapping by the TAE causes the saturation.

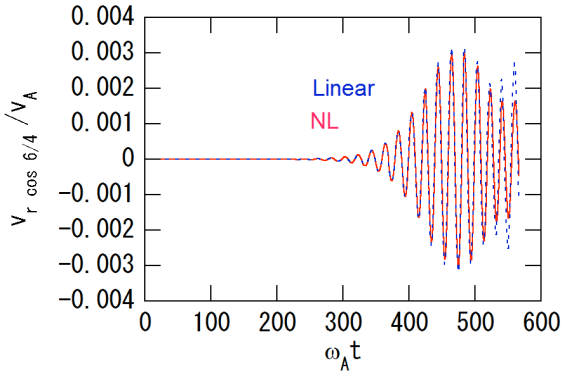

Fig.3 Comparison of radial velocity evolution for the linear-MHD and the nonlinear MHD runs using the cosine part of m/n=6/4 harmonic at r/a=0.42 for β_{h0}=1.5%.

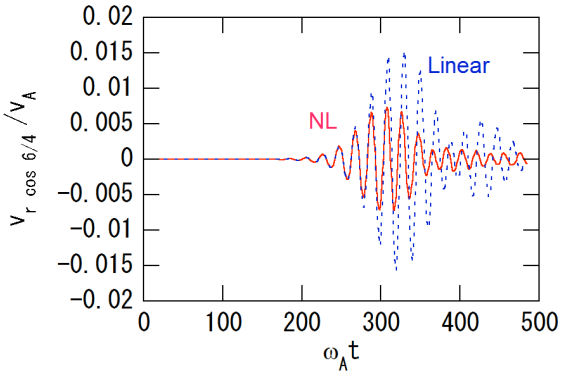

Fig.4 Comparison of radial velocity evolution for the linear-MHD and the nonlinear MHD runs using the cosine part of m/n=6/4 harmonic at r/a=0.42 for β_{h0}=2.0%.

3.2. Physics mechanism of saturation level reduction

In this subsection, we discuss the physics mechanism that reduces the TAE saturation level. We focus on the energy dissipation that is the viscous heating and the Joule heating. They are respectively in proportion to viscosity ν and resistivity η. We analyzed the time evolution of the energy and energy dissipation for each toroidal mode number n for the initial central energetic-ion beta $\beta_{h0} = 1.7\%$. For this case, the TAE saturation level in the nonlinear MHD simulation is reduced by nearly half to $v_r / v_A \sim 6 \times 10^{-3}$, while it is $v_r / v_A \sim 1.0 \times 10^{-2}$ for the linear-MHD simulation.

We analyzed the evolution of the energy dissipation for each toroidal mode number n

$$D_n = \int [\nu \rho_0 \omega_n^2 + \frac{4}{3} \nu \rho_0 (\nabla \cdot \mathbf{v}_n)^2 + \eta \delta \mathbf{j}_n \cdot \mathbf{j}_n] \, dV ,$$

where ω is the vorticity, $\mathbf{j}$ is the current density, and $\delta\mathbf{j}$ is the fluctuation current density. In Fig. 5 the evolution of $\gamma_{d\,n} = D_n / 2E_4$ and $\gamma_{d\,ALL} = D_{ALL} / 2E_4$ are compared with $\gamma_{d\,\mathrm{lin}} = D_4 / 2E_4$ in the relevant linear-MHD simulation. Here, E_4 is the MHD fluctuation energy with toroidal mode number n=4, and D_{ALL} is the summation of D_n over all the toroidal mode numbers. The total damping rate $\gamma_{d\,ALL}$, in the nonlinear MHD simulation, is clearly greater than the n=4 TAE damping rate $\gamma_{d\,\mathrm{lin}}$ in the linear-MHD simulation. This explains why the saturation level is reduced by the MHD nonlinearity. Figure 6 is a schematic diagram of the energy transfer. In the linear MHD simulation, energy is transferred from the energetic-particles to the TAE and dissipates to thermal energy. In the nonlinear MHD simulation, there appears another energy flow channel from the TAE to the n=0 and higher-n modes through nonlinear coupling. The energy of the nonlinear modes also dissipates to thermal energy leading to the enhanced dissipation and increased damping rate. This results in the lower saturation level in the nonlinear MHD simulation. The reduction of the saturation

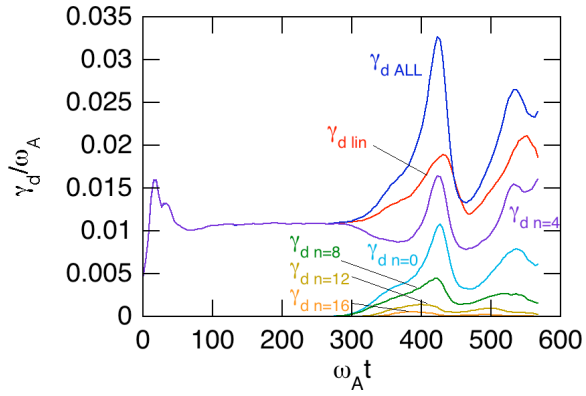

Fig.5 Evolution of damping rate for each toroidal mode number and total damping rate in the nonlinear MHD simulation, and damping rate in the linear-MHD simulation for β_{h0}=1.7%.

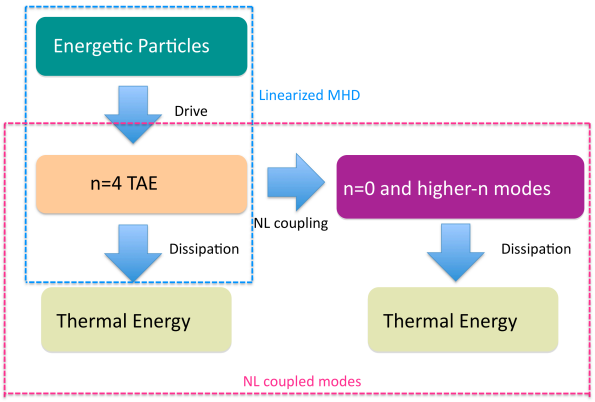

Fig.6 Schematic diagram of energy transfer from energetic particles to TAE and from TAE to n=0 and higher-n modes through nonlinear coupling, and of dissipation from TAE and nonlinear modes.

amplitude by the nonlinear MHD effects but with dissipation reduced to 1/4 with $\nu = \nu_n = 2.5\times10^{-7} v_A R_0$ and $\eta = 2.5\times10^{-7}\mu_0 v_A R_0$ was also demonstrated in Ref. 13.

3.3. Spatial profile and evolution of nonlinearly generated *n*=0 mode

Let us examine the spatial profiles and the evolution of the nonlinearly generated modes. We have analyzed the spatial profiles of the *n*=0 poloidal flow for different times of the nonlinear MHD simulation with $\beta_{h0} = 2.0\%$. The radial velocity evolution for *n*=4 mode was already shown in Fig. 4. The spatial profile of the *n*=0 poloidal flow at $\omega_A t = 189$ is shown in Fig. 7. The n=0 poloidal flow profile remains constant during the linear phase of the TAE instability. The profile peaks at the maximum position of the TAE mode amplitude. The largest harmonics are the *m*/*n*=0/0 and 1/0 cosine ($\propto \cos\vartheta$) harmonics. The evolution of the 0/0 harmonic of the poloidal flow, namely the zonal flow, is shown in Fig. 8 along with the 1/0 sine harmonic of the pressure fluctuation. As can be seen in Fig. 8, the zonal flow and the pressure oscillate with the same frequency after the saturation of the instability. This oscillation is a geodesic acoustic mode (GAM) because the frequency of the oscillation $\omega = 0.11\omega_A$ is close to the theoretical GAM frequency $\omega_{\mathrm{GAM}} = \omega_A\sqrt{\gamma\beta_{\mathrm{bulk}}(1+1/2q^2)} = 0.12\omega_A$ [17, 18] with $\gamma = 5/3$, $\beta_{bulk} = 6.5\times10^3$, and $q = 1.37$. Furthermore, the coupling between the zonal flow and the 1/0 sine harmonic of the pressure fluctuation is consistent with the GAM theory.

4. Simulation of Alfvén eigenmode bursts with nonlinear MHD effects

The hybrid simulation code MEGA has been extended to incorporate energetic-particle source, loss, and collisions. The energetic particles are simulated using the δf particle-in-cell method

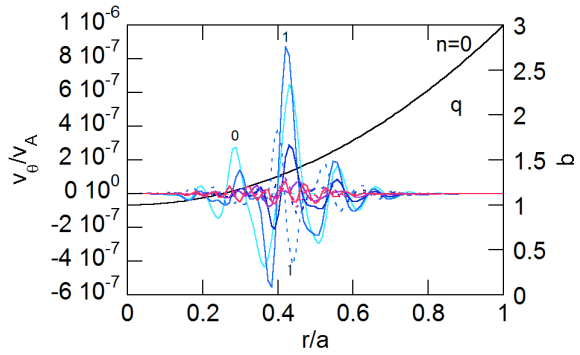

Fig.7 Spatial profile of each poloidal harmonic of the poloidal flow with n=0 during the linearly-growing pahse of the TAE instability at $\omega_A t = 189$ for β_{h0}=2.0%. Solid (dashed) lines show $\cos(m\vartheta)$ [$\sin(m\vartheta)$] harmonics with poloidal mode number m labelled in the figure.

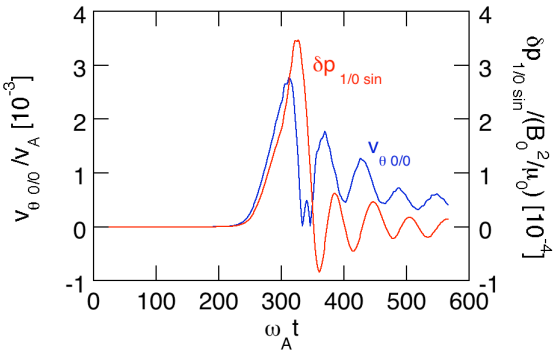

Fig.8 Time evolution of the zonal flow and pressure fluctuation for β_{h0}=2.0%.

with time-dependent equilibrium distribution function f_0. We performed the simulation of toroidal Alfvén eigenmode (TAE) bursts with parameters similar to a TFTR experiment [2]. The parameters are, a=0.75m, R_0=2.4m, B=1T, beam injection energy is 110keV, and NBI power is 10MW. Both the bulk and beam ions are deuterium. The safety factor profile is assumed as the same as Ref. 1, $q(r) = 1.2 + 1.8(r/a)^2$. The slowing-down time is assumed to be 100ms. The beam velocity is purely parallel to the magnetic field to model the parallel beam injection. The pitch-angle scattering is neglected.

The time evolution of radial magnetic field using the cosine part of the dominant harmonics (m/n=4/2 and 5/3) at the peak locations is shown in Fig. 9. The TAEs with toroidal mode numbers n=2 and 3 are dominant in the simulation results. We see the synchronized TAE bursts with a time interval 2.6ms. The time evolution of stored energy for co- and counter-beams is shown in Fig. 10. The beam ion losses take place associated with the TAE bursts. The loss for the counter-beam at each burst amounts to a half of the increase in stored energy during the burst interval. The asymmetry in beam ion loss between the co- and counter-beams may arise from the fact that the counter-beam (co-beam) interacts primarily with the TAE poloidal harmonic m+1 (m) when the major poloidal harmonics are m and m+1. As the m+1 harmonic is located at the outer side in the poloidal plane, the counter-beam ion loss is more easy to take place.

5. Summary and Discussion

The nonlinear MHD effects on the evolution of the Alfvén eigenmode were investigated with hybrid simulations of an MHD fluid interacting with energetic particles. To clarify the role of

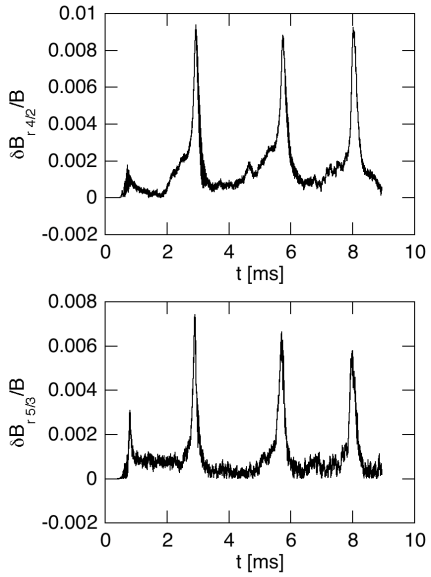

Fig.9 Time evolution of radial magnetic field fluctuation amplitude using the cosine part of the dominant harmonics (m/n=4/2 and 5/3) at the peak locations.

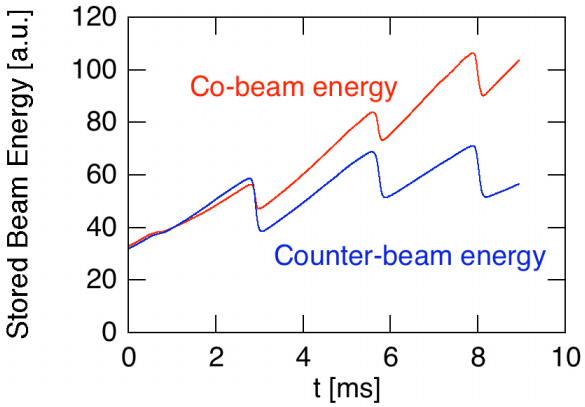

Fig.10 Time evolution of stored energy for co- and counter-beams.

the MHD nonlinearity, the nonlinear MHD results were compared with results from a reduced model, where only linear MHD equations were solved together with a nonlinear response of the energetic particles. Specifically, we studied the evolution of an n=4 TAE mode destabilized by its resonant interaction with energetic particles in a tokamak plasma. When the TAE saturation level is $\delta B/B \le 10^{-3}$ no significant difference was found between the results of the linear-MHD simulation and the nonlinear MHD simulation. On the other hand, when in the linear-MHD simulation the TAE saturation level is $\delta B/B \sim 10^{-2}$, the saturation level in the nonlinear MHD case is found be reduced to half the result of the linear-MHD simulation. We found that the nonlinearly generated n=0 and the higher-n ($n \ge 8$) modes provide increased energy dissipation that appears crucial for achieving a reduced TAE saturation level. Furthermore, energetic-particle source, loss, and collisions are implemented in the hybrid simulation code. The energetic particles are simulated using the δf particle-in-cell method with a time-dependent equilibrium distribution function f_0. We have presented the first numerical demonstration of Alfvén eigenmode bursts with parameters similar to the TFTR experiment and with MHD nonlinearity retained.

The effect of increased damping due to MHD nonlinearities was discussed in previous works [9, 10]. We found in this work that the total dissipation of all the toroidal mode numbers increases before the saturation of the instability. The increased dissipation leads to the reduction of the saturation amplitude even though the damping rate of the n=4 component, which was the original TAE carrier, slightly decreases before saturation. We emphasize that this is a new picture for the mechanism by which nonlinear MHD effects cause saturation that

is different from the previous works which would predict enhanced damping of the n=4 component.

Another interesting discovery of this work is the excitation of the geodesic acoustic mode (GAM) after the saturation of the TAE instability. In the linearly growing phase of the instability, the zonal fluctuations are matched to the growth of the nonlinear source, with a spatial profile kept constant. When the instability saturates, however, the spatial profile of the zonal fluctuations is no longer matched to the evolution of the nonlinear source. This excites the n=0 MHD waves that includes the GAM. It is evident that the GAM is excited through the nonlinear MHD effect because the n=4 fluctuations of the energetic-particle current density retained in the simulations cannot directly drive the GAM. This excitation mechanism of the GAM is different from the direct destabilization by the energetic particles [19, 20]. We note that the excitation of zonal flow and GAM through the TAE nonlinearity is an interesting phenomenon for burning plasmas since its excitation may lead to improved plasma confinement and to bulk plasma heating through the damping of the GAM.

ACKNOWLEDGMENTS
Numerical computations were performed at the Plasma Simulator (HITACHI SR16000) of National Institute for Fusion Science. This work was supported by a Grant-in-Aid for Scientific Research from the Japan Society for the Promotion of Science (No. 20340165).

References

[1] TODO, Y., BERK, H. L., BREIZMAN, B. N., Phys. Plasmas **10** (2003) 2888.
[2] WONG, K. L., et al., Phys. Rev. Lett. **66** (1991) 1874.
[3] DURST, R. D., et al., Phys. Fluids B **4** (1992) 3707.
[4] BERK, H. L., BREIZMAN, B. N., Phys. Fluids B **2** (1990) 2246.
[5] BERK, H. L., BREIZMAN, B. N., YE, H., Phys. Fluids B **5** (1993) 1506.
[6] FU, G. Y., PARK, W., Phys. Rev. Lett. **74** (1995) 1594.
[7] TODO, Y., et al., Phys. Plasmas **2** (1995) 2711.
[8] WU, Y., et al., Phys. Plasmas **2** (1995) 4555.
[9] BRIGUGLIO, S., ZONCA, F., VLAD, G., Phys. Plasmas **5** (1998) 3287.
[10] TODO, Y., et al., Nuclear Fusion **41** (2001) 1153.
[11] ZONCA, F., ROMANELLI, F., VLAD, G., KAR, C., Phys. Rev. Lett. **74** (1995) 698.
[12] SPONG, D. A., CARRERAS, B. A., HEDRICK, C. L., Phys. Plasmas **1** (1994) 1503.
[13] TODO, Y., BERK, H. L., BREIZMAN, B. N., Nucl. Fusion **50** (2010) 084016.
[14] TODO, Y., SATO, T., Phys. Plasmas **5** (1998) 1321.
[15] TODO, Y., et al., Phys. Plasmas **12** (2005) 012503.
[16] TODO, Y., Phys. Plasmas **13** (2006) 082503.
[17] WINSOR, N., JOHNSON, J. L., DAWSON, J. M., Phys. Fluids **11** (1968) 2448.
[18] HASSAM, A. B., DRAKE, J. F., Phys. Fluids B **5** (1993) 4022.
[19] BERK, H. L., et al., Nucl. Fusion **46** (2006) S888.
[20] FU, G. Y., Phys. Rev. Lett. **101** (2008) 185002.